Peptide Bond Conformation in Peptides and Proteins Probed by Dipolar Coupling-Chemical Shift Tensor Correlation Solid-State NMR

Dwaipayan Mukhopadhyay, Chitrak Gupta, Theint Theint, and Christopher P. Jaroniec*

Department of Chemistry and Biochemistry, The Ohio State University,
Columbus, OH, 43210

* E-mail: jaroniec.1@osu.edu

Abstract

Multidimensional magic-angle spinning solid-state NMR experiments are described that

permit cis and trans peptide bonds in uniformly ¹³C, ¹⁵N-labeled peptides and proteins to be

unambiguously distinguished in residue-specific manner by determining the relative

orientations of the amide ¹³C' CSA and ¹H-¹⁵N dipolar coupling tensors. The experiments are

demonstrated for model peptides glycylglycine and 2,5-diketopiperazine containing trans and

cis peptide bonds, respectively. Subsequently, the measurements are extended to two

representative proteins that contain exclusively trans peptide bonds, microcrystalline B3

immunoglobulin domain of protein G and Y145Stop human prion protein amyloid fibrils, to

illustrate their applicability to a wide range of protein systems.

Keywords: protein structure; peptide bond conformation; tensor correlation; magic-angle

spinning solid-state NMR

2

1. Introduction

Magic angle spinning (MAS) solid-state nuclear magnetic resonance (NMR) has become a widely used technique for the elucidation of atomic-level structure of biological macromolecules [1-8]. Such structural studies typically rely upon experimental restraints on interatomic distances and backbone and side-chain dihedral angles derived from measurements of isotropic chemical shifts, chemical shift anisotropies (CSAs), magnitudes of nuclear dipolar couplings and relative orientations of dipolar coupling and/or CSA tensors [9], and, more recently, paramagnetism-based restraints including pseudocontact shifts and paramagnetic relaxation enhancements [10-12].

A multitude of MAS solid-state NMR tensor correlation techniques, designed to directly measure dihedral angles in uniformly 13 C, 15 N-enriched peptides and proteins, have been developed to date [13-26], with primary focus on determining backbone torsion angles ϕ (C'_{i-1}-N_i-C α_i -C'_i) and ψ (N_i-C α_i -C'_i-N_{i+1}) which vary significantly for different secondary structures. In contrast, analogous tensor correlation experiments that are capable of directly probing the peptide bond conformation, defined by torsion angle ω (C α_{i-1} -C'_{i-1}-N_i-C α_i), on a residue-by-residue basis have not been reported; although, we note here that conformations of specific peptide bonds in selectively 13 C-labeled peptide and peptoid molecules have been characterized previously using solid-state NMR by determining the relative orientation of the 13 C' CSA tensor and the dipolar coupling between that 13 C' and a 13 C α spin of the adjacent amino acid residue [27] and the magnitude of the dipolar coupling between two 13 C α nuclei located in neighboring residues [28].

One reason for the somewhat limited focus on directly probing peptide bond ω torsion angles in peptides and proteins by NMR techniques is that the peptide bonds are almost always present in their most thermodynamically stable *trans* ($\omega \sim 180^{\circ}$) conformation, while the less favorable cis ($\omega \sim 0^{\circ}$) conformation or other conformations that are intermediate between cis

and trans are relatively rare by comparison [29]. Indeed, a comprehensive survey carried out for a set of nearly six hundred non-redundant proteins with high-resolution X-ray crystal structures deposited in the PDB [30,31], containing over 150,000 peptide bonds, identified only 429 cis peptide bonds altogether (~90% of these corresponded to Xaa-Pro and ~10% to Xaanon-Pro, where Xaa is any amino acid). Within the same dataset only ~5.2% of all Xaa-Pro and ~0.03% of all Xaa-non-Pro peptide bonds were found to adopt the cis conformation. Interestingly, however, the same study noted a significant correlation between the number of cis peptide bonds identified and the resolution of the crystal structure (e.g., Xaa-non-Pro cis peptide bonds were encountered approximately four times more frequently in structures with <2.0 Å resolution compared to those with ≥ 2.5 Å resolution), leading to the suggestion that a non-negligible number of cis peptide bonds in proteins may not have been recognized as such during the course of structure determination, particularly for lower resolution structures [30,31]. Additionally, it appears that, in cases where they have been unambiguously identified, Xaa-non-Pro cis peptide bonds may be of particular significance for biological function and mechanism, given that they tend to be located at or in the immediate vicinity of functionally important sites [32-36]. For example, in the structural study of the GyrA intein the peptide bond at the extein-intein boundary was found to be present in a highly strained cis conformation, likely providing part of the driving force required for isomerization and cleavage [35,36].

Xaa-Pro *cis* and *trans* peptide bonds in peptides and proteins can be readily distinguished by solution and solid-state NMR on the basis of 13 Cβ and 13 Cγ chemical shifts of the proline residue [37-40]. In contrast, no similar chemical shift-based approaches are available to unambiguously identify the rare, but potentially functionally relevant, Xaa-non-Pro *cis* peptide bonds. While, Xaa-non-Pro *cis* peptide bonds in proteins could in principle be detected from solution NMR measurements of 1 H α - 1 H α NOEs between adjacent amino acid

residues [41] or from analogous measurements of ¹Hα-¹Hα and/or ¹³Cα-¹³Cα dipolar couplings by MAS solid-state NMR, such measurements may be difficult or impossible to perform in a quantitative manner in either protonated or deuterated uniformly ¹³C, ¹⁵N-enriched proteins. Here, we describe multidimensional MAS solid-state NMR experiments that enable the unambiguous identification of cis and trans peptide bonds in uniformly ¹³C, ¹⁵N-labeled peptides and proteins in residue-specific fashion by determining the relative orientation of two tensorial interactions: the ¹³C' CSA of a selected amino acid residue and the amide ¹H-¹⁵N dipolar coupling of the following residue. These experiments build upon previous solid-state NMR tensor correlation techniques developed to measure backbone and side-chain dihedral angles [13-26] as well as relative orientations of dipolar and CSA tensorial interactions at specific sites in peptides and proteins [42]. The experiments are first demonstrated on two peptides glycylglycine (GG) and 2,5-diketopiperazine (DKP), which serve as models for trans and cis peptide bonds, respectively (Fig. 1). Subsequently, the experiments are extended toward two representative proteins, microcrystalline B3 immunoglobulin domain of protein G (GB3) and Y145Stop human prion protein (huPrP23-144) amyloid fibrils, to illustrate their applicability to a wide range of protein systems.

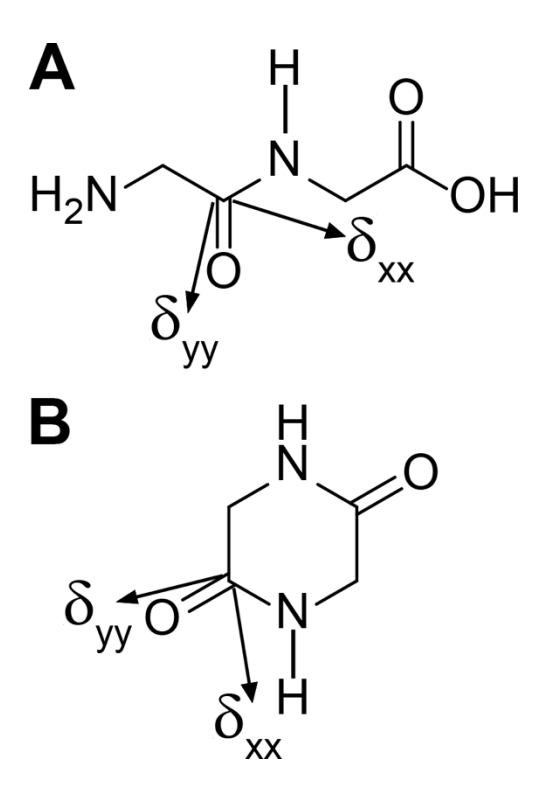


Figure 1. Model peptides (A) glycylglycine and (B) 2,5-diketopiperazine containing peptide bonds with *trans* and *cis* conformation, respectively. The 15 N- 1 H dipolar coupling and 13 C'CSA interactions within the peptide bond of interest are indicated. For the 15 N- 1 H dipolar coupling tensor the unique principal axis coincides with the 15 N- 1 H bond. For the 13 C'CSA tensor the approximate orientations of the δ_{xx} and δ_{yy} principal axes in the molecular frame are indicated (the angle between the δ_{xx} axis and the C'-N bond is \sim 40°), with the δ_{zz} axis being perpendicular to the peptide plane [43-45]. The relative orientation of the 13 C'CSA and 15 N- 1 H dipolar coupling tensors depends on the peptide bond torsion angle ω .

2. Materials and methods

2.1. U-¹³C, ¹⁵N-glycylglycine

U-13C, 15N-labeled glycylglycine was prepared via standard Fmoc solid-phase peptide synthesis using U-13C, 15N-Fmoc-glycine purchased from Cambridge Isotope Labs. 2.00 g of Wang resin (AAPPTec) was washed with dichloromethane (DCM) for 30 min and with 10% (v/v) solution of dimethylformamide (DMF) in DCM for 30 min. 200.6 mg of hydroxybenzotriazole monohydrate (HOBt·H₂O) and 20.7 mg 4-dimethylaminopyridine (DMAP) were added to 400 mg of U-13C, 15N-Fmoc-glycine and dissolved in minimum volume of DMF (~3 mL), followed by addition of 200 µL of N,N'-diisopropylcarbodiimide (DIC). This mixture was then added to the resin and shaken for 14 h, after which 0.1 mL pyridine and 120 μL acetic anhydride were added and the mixture shaken for an additional 30 min. The liquid was removed and the resin washed alternately with DCM and DMF four times. The resin was then dried and washed once more with DMF, followed by addition of 20% (v/v) piperidine in DMF and shaking for 30 min. After drying the resin, a Kaiser test was done confirming presence of free amine. The resin was then washed alternately with DCM and DMF four times, dried, and washed with 10% (v/v) DMF in DCM. A mixture of HOBt·H₂O, DMAP and U-¹³C, ¹⁵N-Fmoc-glycine and DIC in DMF was then prepared as described above, added to the resin and shaken for 8 h, followed by the alternating wash procedure in DCM and DMF. After the resin was dried, 50% (v/v) trifluoroacetic acid (TFA) in DCM was added and the resin shaken for 2 h. The filtrate was collected, and DCM and TFA removed by drying under vacuum at 60 °C for 2 h and then at 35 °C overnight, followed by air drying at ambient temperature for 24 h. The resulting residue was then combined with 20% (v/v) piperidine in DMF and shaken for 24 h, followed by air drying. The crude GG product was dissolved in water and purified by using reversed-phase HPLC (Waters 1525 HPLC system) with a preparative C18 column, gradient elution with water/acetonitrile containing 0.01% (v/v) TFA, where the H₂O

concentration was varied from 95% to 70% in 20 min, and a flow rate of 8 mL/min. The identity of the final purified GG was confirmed by routine ESI mass spectrometry and ¹H and ¹³C NMR, with additional comparison to corresponding data obtained for a commercially available glycylglycine (Bachem) reference. For the solid-state NMR experiments the U-¹³C, ¹⁵N-glycylglycine was lyophilized, crystallized from aqueous solution as a hydrochloride salt [46], and transferred to a Varian 3.2 mm zirconia rotor.

$2.2.~U-^{13}C$, $^{15}N-2$, 5-diketopiperazine

U-¹³C,¹⁵N-labeled 2,5-diketopiperazine was synthesized by using a microwave-assisted protocol described in the literature [47]. Briefly, 250 mg of U-¹³C,¹⁵N-glycine (Cambridge Isotope Labs) was dissolved in 2 mL of DMF in a 10 mL microwave reaction vessel and placed in a CEM Discover microwave reactor with a set point temperature of 210 °C and a hold time of 30 min. The reaction mixture, which consisted primarily of the desired DKP product, was purified using reversed-phase HPLC under conditions described above for GG, and the identity of the final purified DKP was confirmed by ¹H and ¹³C NMR with additional comparisons to corresponding data obtained for a commercially available 2,5-diketopiperazine (Sigma-Aldrich) reference. For the solid-state NMR experiments U-¹³C,¹⁵N-2,5-diketopiperazine was lyophilized, crystallized from aqueous solution and transferred to a Varian 3.2 mm zirconia rotor.

2.3. ¹³C, ¹⁵N-labeled proteins

Protein samples described in detail in our earlier studies were used including U-¹³C, ¹⁵N-labeled B3 immunoglobulin binding domain of protein G [48], and ¹³C, ¹⁵N-enriched Y145Stop human prion protein amyloid fibrils generated from protein expressed using the 1,3-¹³C-glycerol labeling scheme [49].

2.4. NMR data acquisition and processing

All NMR experiments were performed on a three-channel Varian VNMRS spectrometer operating at frequencies of 499.8 MHz for 1 H, 125.7 MHz for 13 C, and 50.6 MHz for 15 N, equipped with a 3.2 mm BioMAS 1 H- 13 C- 15 N probe. The MAS frequency was set to 9.921 kHz \pm 3 Hz and the effective sample temperature was maintained at \sim 5°C for all experiments.

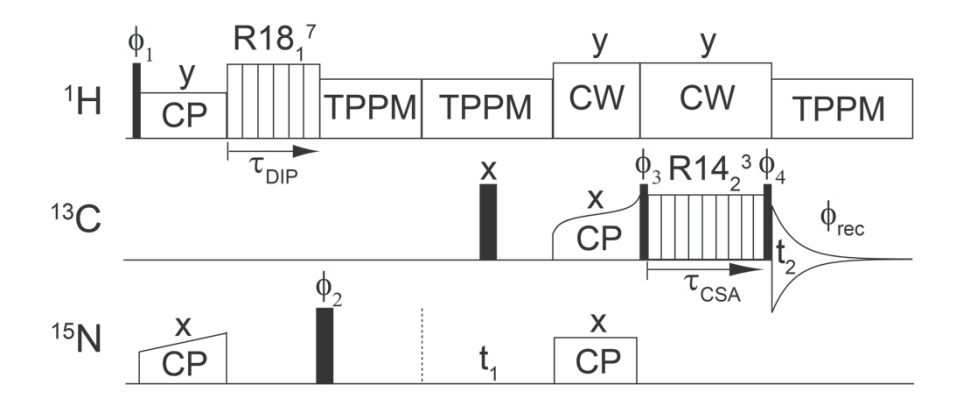


Figure 2. General pulse scheme used to record the ¹H-¹⁵N dipolar/¹³C'CSA tensor correlation spectra. Narrow and wide black rectangles correspond to 90° and 180° pulses, respectively, and crosspolarization (with appropriate shapes) and CW and TPPM ¹H decoupling periods are indicated. The ¹H-¹⁵N dipolar coupling and ¹³C'CSA interactions are reintroduced by using the γ -encoded R18₁⁷ and R14₂³ sequences, incremented during τ_{DIP} and τ_{CSA} , respectively, while the ^{15}N and ^{13}C isotropic chemical shifts are encoded during t₁ and t₂, respectively. Additional description of the R-symmetry sequences is provided in the text. Briefly, for the 9.921 kHz MAS rate ($\tau_r = 100.8 \mu s$) employed in this study, one complete cycle of the R18₁⁷ sequence consists of 18 π pulses with 5.6 μ s length (~89.3 kHz field) applied on the ¹H channel within one rotor period in phase-altered (-70°, +70°) manner, and one complete cycle of the R14₂³ sequence consists of 14 π pulses with 14.4 μ s length (~34.7 kHz field) applied on the ¹³C channel within two rotor periods in phase-altered (-38.57°, +38.57°) manner. Note that for the model peptides the spectra were recorded without ^{15}N chemical shift evolution (i.e., $t_1 = 0$) in either pseudo-3D (independent ¹H-¹⁵N dipolar coupling and ¹³C' CSA dimensions) or pseudo-2D manner (concurrent ¹H-¹⁵N dipolar coupling and ¹³C' CSA evolution achieved by simultaneously incrementing τ_{DIP} and τ_{CSA}) as described in the text. For protein samples, the spectra were recorded in pseudo-3D manner with ¹⁵N chemical shift evolution during t₁ and concurrent ¹H-¹⁵N dipolar coupling/ 13 C' CSA evolution. Phase cycling: $\phi_1 = 8(x), 8(-x); \phi_2 = 2(x,y); \phi_3 = 4(y), 4(-y); \phi_4 = 2(-y), 2(y);$ was achieved by changing the phase of the 15 N spin-lock pulse during 15 N- 13 C' CP from x to y according to the States method [50].

Correlation of the ¹⁵N-¹H dipole and ¹³C'CSA tensors as well as encoding of up to two isotropic chemical shift dimensions was performed by using variations of the pulse sequence

shown in Fig. 2. The carrier positions were as follows: 4.7 ppm for ¹H, 120 ppm for ¹⁵N, and 170 ppm (GG and DKP) or 175 ppm (proteins) for ¹³C. Recycle delays of 2.5 s were used for all experiments except those involving DKP, for which the recycle delay was 10 s due to the longer ¹H T₁. The 90° pulse lengths were 2.5 μs for ¹H, 5 μs for ¹³C, and 5.5 μs for ¹⁵N. ¹H-¹⁵N cross-polarization (CP) was achieved using a ~45 kHz ¹H field and a ~35 kHz ¹⁵N field (with a linear ramp), with a contact time of 1.2 ms. Both CW and TPPM [51] ¹H decoupling was used as indicated in the pulse scheme with fields of ~100 kHz and ~71 kHz, respectively. Selective ¹⁵N-¹³C' magnetization transfer was achieved using SPECIFIC CP [52], with a ~35 kHz ¹⁵N field, a ~25 kHz ¹³C field (with a tangent ramp), and a 3.5 ms contact time. The details of the R18₁⁷ and R14₂³ sequences used to recouple the ¹⁵N-¹H dipolar coupling and ¹³C' CSA interactions are provided in Fig. 2, and the dwell times and total durations of these frequency dimensions, which were varied for the different experiments, are provided in the corresponding figure captions.

Data were processed in NMRPipe [53]. For GG and DKP a squared cosine bell window was used for apodization for the isotropic chemical shift dimensions, while for the protein samples a 60° shifted sine bell window was used. The time-domain dephasing profiles under the recoupled ¹⁵N-¹H dipolar coupling and ¹³C' CSA interactions were extracted either from a series of 1D ¹³C spectra (GG and DKP) or from a series of 2D ¹⁵N-¹³C' chemical shift correlation spectra (proteins), using python scripts in nmrglue [54]. These time-domain data were imported into Origin 9.0, zero-filled to 2048 points and Fourier transformed without applying any line-broadening to generate the 1D frequency-domain lineshapes reporting on combined evolution under the recoupled ¹⁵N-¹H dipolar and ¹³C' CSA interactions. The 2D ¹⁵N-¹H dipolar/¹³C' CSA frequency-domain lineshapes for GG and DKP were obtained after zero-filling to 512 points in each dimension.

2.5. Simulations of NMR spectra

A molecular model corresponding to a peptide bond fragment consisting of three coupled spins (¹H, ¹⁵N and ¹³C') as well as the Cα and O atoms was built with the following bond distances and angles, N-H: 1.04 Å, N-C': 1.33 Å, C'-Cα: 1.52 Å, H-N-C': 119.5°, N-C'-O: 123.2°, and O-C'-Cα: 121.2°. For the *trans* conformation of the peptide bond, corresponding to GG, the H-N-C'-O torsion angle was set to 180°, while for the *cis* conformation, corresponding to DKP, the H-N-C'-O torsion angle was set to 0°. ¹³Cα was not considered as part of the coupled spin system in the simulations of ¹⁵N-¹H dipole/¹³C'CSA correlation spectra since the R18₁⁷ and R14₂³ sequences do not recouple homonuclear dipolar interactions.

Numerical simulations of the NMR spectra were performed using the SPINEVOLUTION software package [55], with 1 H Larmor frequency of 499.8 MHz, MAS frequency of 9.921 kHz, and other acquisition and processing parameters corresponding to their experimental values. The ZCW987 α , β angle set and three γ angle values were used to generate the powder averaged spectra. All the dipolar coupling magnitudes were obtained directly from the corresponding bond lengths in the molecular model, while the 13 C' CSA tensor parameters ($\delta = 82.3$ ppm and $\eta = 0.84$) and orientation in the molecular frame corresponded to the previously reported experimental values for GG [43]. Since the R18 $_{1}^{7}$ and R14 $_{2}^{3}$ sequences recouple both the heteronuclear dipolar couplings and CSA for the irradiated spin [56], and in our experiments efficient 15 N decoupling was not feasible during the R14 $_{2}^{3}$ period due to probe limitations, the simulations also included the amide 1 H CSA ($\delta = 8.9$ ppm and $\eta = 0.75$) [42] during the R18 $_{1}^{7}$ 15 N- 1 H dipolar evolution period and the 13 C'- 15 N dipolar coupling during the R14 $_{2}^{3}$ 13 C' CSA evolution period. Finally, for best agreement between the experimental and simulated spectra, the simulations also included the effects of transverse relaxation during the 15 N- 1 H dipolar and 13 C' CSA evolution periods.

3. Results and discussion

3.1. Pulse sequence description

The pulse scheme shown in Fig. 2 was used to record the $^{1}H^{-15}N$ dipolar/ $^{13}C'$ CSA tensor correlation spectra. Briefly, following $^{1}H^{-15}N$ CP, the resulting amide ^{15}N magnetization was allowed to evolve during the period τ_{DIP} primarily under the $^{15}N^{-1}H$ dipolar interaction recoupled by using the R18 $_{1}^{7}$ sequence (see below). This was followed by a period of ^{15}N isotropic chemical shift evolution during t_{1} (used here only for the protein samples to generate residue-specific correlations, but not necessary for GG and DKP), and subsequently SPECIFIC CP [52] was employed to transfer the ^{15}N magnetization to the $^{13}C'$ of the preceding residue. The $^{13}C'$ magnetization was then allowed to evolve during the period τ_{CSA} primarily under the $^{13}C'$ CSA interaction recoupled by using the R14 $_{2}^{3}$ sequence, and finally detected during t_{2} . Note that the τ_{DIP} and τ_{CSA} periods were incremented either independently or concurrently, as discussed in detail in the text.

The 15 N- 1 H dipolar coupling and 13 C' CSA interactions were reintroduced under MAS by using well-known R-symmetry sequences—R18 $_1$ 7 and R14 $_2$ 3 applied during the periods τ_{DIP} and τ_{CSA} , respectively, as noted above—described in detail previously [42,56-60]. In general, a RN $_n^{\nu}$ sequence consists of N basic elements R that each rotate the nuclear spins by 180° (single π pulse in our case), applied as phase-alternated pairs with an overall phase shift $\phi = \pi \nu/N$ within the interval $n\tau_r$, where τ_r is the rotor period, repeated multiple times as required [56]:

$$RN_n^{\nu} = \left[R_{\phi} R_{-\phi} \right]_{N/2} \tag{1}$$

In the interaction frame of the applied RF irradiation, the first-order average Hamiltonian for the internal spin interactions during a RN_n^{ν} sequence is given by [56]:

$$\overline{H}_{int} = \sum_{\Lambda,l,m,\lambda,\mu} \overline{H}_{lm\lambda\mu}^{\Lambda} = \sum_{\Lambda,l,m,\lambda,\mu} \kappa_{m\lambda\mu} A_{lm}^{\Lambda}(\Omega_{PR}) d_{m0}^{l}(\beta_{RL}) T_{\lambda\mu}^{\Lambda}$$
(2)

where Λ indicates the specific spin interaction (i.e., CSA, heteronuclear dipolar coupling, etc.), l is the space rank of interaction Λ with m=-l,-l+1,...,+l being the space rotational component, and λ is the spin rank of interaction Λ with $\mu=-\lambda,-\lambda+1,...,+\lambda$ being the spin rotational component. $\kappa_{m\lambda\mu}$ is the scaling factor due to RF irradiation, $A_{lm}^{\Lambda}(\Omega_{PR})$ is the spatial component of the interaction that depends on the Euler angles $\Omega_{PR}=\{\alpha_{PR},\beta_{PR},\gamma_{PR}\}$ connecting the principal axis system to the rotor-fixed frame, $d_{m0}^{l}(\beta_{RL})$ is the Wigner matrix element dependent on the angle β_{RL} connecting the rotor-fixed frame to the lab frame, and $T_{\lambda\mu}^{\Lambda}$ is the spin component of the interaction.

For a RN_n^{ν} sequence, symmetry imposes the following selection rule for the first-order average Hamiltonian terms, which enables selective recoupling of the different nuclear spin interactions based on their rotational properties [56]:

$$\overline{H}_{lm\lambda\mu}^{\Lambda} = 0 \text{ if } mn - \mu\nu \neq \frac{N}{2}Z_{\lambda}$$
 (3)

where Z_{λ} is an integer with the same parity as λ . Consequently, both the R18₁⁷ and R14₂³ sequences utilized in this study provide γ -encoded recoupling of the CSA and heteronuclear dipolar coupling interactions for the irradiated spin (l=2 and $\lambda=1$ for both interactions), with selection of the $\{l,m,\lambda,\mu\}=\{2,-2,1,1\}$ and $\{2,2,1,-1\}$ terms, and concurrent suppression of homonuclear dipolar couplings and isotropic chemical shifts [42,56-60]. Note that during R18₁⁷ the amide ¹⁵N magnetization evolves primarily under its dipolar coupling to the directly bonded amide ¹H, since the magnitude of this interaction significantly exceeds the amide ¹H CSA as well as couplings between the amide ¹H and other spins. Likewise, the ¹³C'-CSA is the dominant interaction during R14₂³ evolution, given that the recoupled ¹³C'-¹⁵N dipolar interaction is much smaller in magnitude and that couplings to ¹H nuclei are suppressed by using high-power proton decoupling.

3.2. Recoupling of heteronuclear dipolar and CSA interactions by R-symmetry sequences

Prior to recording the tensor correlation spectra, control experiments were carried out for the model peptides GG and DKP using the pulse scheme in Fig. 2, with either the R18₁⁷ or the R14₂³ period incremented, in order to quantitatively assess the performance of ¹H-¹⁵N dipolar and ¹³C' CSA recoupling under our experimental conditions. Fig. 3A shows the ¹H-¹⁵N dipolar trajectory in the time domain for GG, obtained by incrementing the R18₁⁷ period up to ~2 ms, with the corresponding frequency-domain dipolar lineshape shown in Fig. 3C. The trajectory shows pronounced oscillations indicative of efficient γ -encoded dipolar recoupling, and the best-fit simulations are consistent with a ¹H-¹⁵N dipolar coupling constant of ~10.8 kHz and R18₁⁷ scaling factor of ~0.18 [58] as expected (corresponding data for DKP are shown in SI Fig. S1A and S1C). Fig. 3B shows the time-domain ¹³C' CSA trajectory for GG obtained by incrementing the R1423 period up to ~3.5 ms, with the corresponding CSA lineshape in the frequency domain shown in Fig. 3D and data for DKP shown in SI Fig. S1B and S1D. Since in peptides and proteins some site-to-site variation in the ¹³C' CSA magnitude and orientation in the molecular frame is expected [61-63], for simplicity, rather than attempting to fit these parameters individually for each site, all calculations performed in this study were carried out with the 13 C' CSA parameters fixed to the values previously reported for GG ($\delta = 82.3$ ppm and $\eta = 0.84$) [43]. Consequently, the best-fit simulations for GG are of particularly high quality and consistent with the known ¹³C' CSA tensor parameters and R14₂³ scaling factor of ~0.3 [58,60]. On the other hand, while the fit quality for DKP is not as high as for GG, the use of the fixed GG ¹³C' CSA parameters in the simulations is nevertheless sufficient to readily distinguish between cis and trans peptide bond conformations in the context of the tensor correlation experiments discussed below.

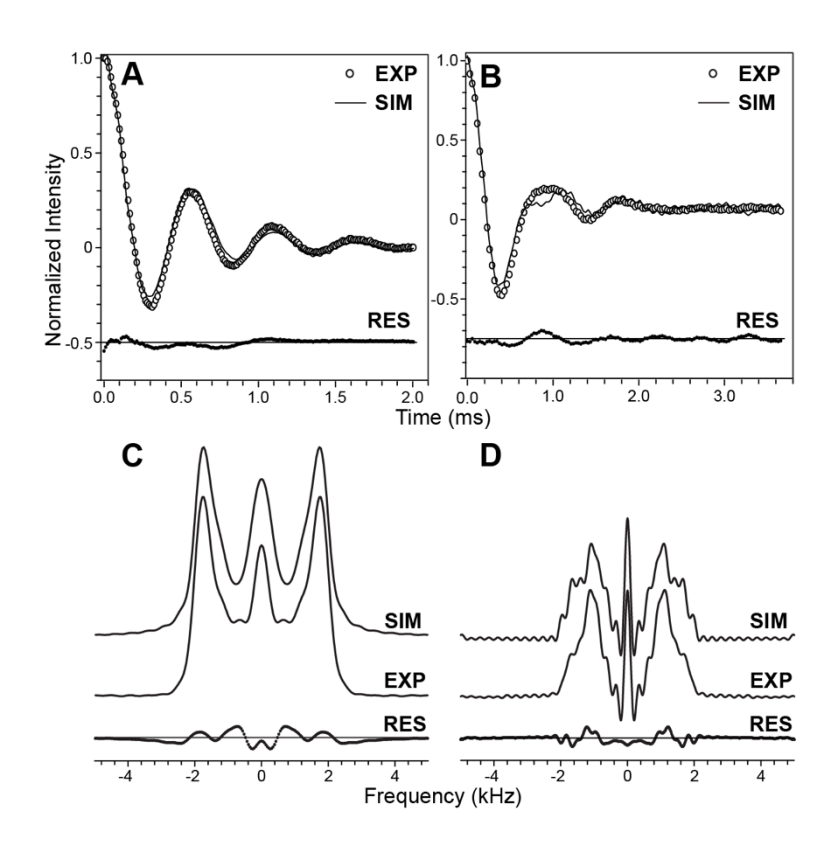


Figure 3. (A) Time-domain ${}^{1}\text{H-}{}^{15}\text{N}$ dipolar trajectory for GG obtained by using the pulse scheme in Fig. 2 with t_1 and τ_{CSA} set to zero and the duration of the R18₁⁷ (τ_{DIP}) period incremented in units of 11.2 μs corresponding to two π pulses with -70°, +70° phase alternation. (B) Time-domain ${}^{13}\text{C}'$ CSA trajectory for GG obtained by using the pulse scheme in Fig. 2 with t_1 and τ_{DIP} set to zero and the duration of the R14₂³ (τ_{CSA}) period incremented in units of 28.8 μs corresponding to two π pulses with -38.57°, +38.57° phase alternation. In panels (A) and (B) the experimental trajectories are shown as open circles and best-fit simulations as solid lines, with the residuals shown beneath the trajectories. (C,D) Experimental and simulated ${}^{1}\text{H-}^{15}\text{N}$ dipolar (C) and ${}^{13}\text{C}'$ CSA (D) lineshapes in the frequency domain corresponding to the time-domain trajectories in panels (A) and (B), respectively.

3.3. Tensor correlation experiments for model peptides

For GG and DKP, as well as other peptides with well-resolved 13 C' resonances in a 1D spectrum, the 1 H- 15 N dipolar/ 13 C' CSA tensor correlation spectra can be recorded within reasonable measurement times in a pseudo-3D manner with complete 1 H- 15 N dipolar and 13 C' CSA frequency dimensions by using the pulse scheme in Fig. 2 with no 15 N chemical shift evolution (i.e., $t_1 = 0$) while independently incrementing the R18 $_1$ 7 and R14 $_2$ 3 blocks during τ_{DIP} and τ_{CSA} , respectively. In Fig. 4A and 4B we show the experimental 1 H- 15 N dipolar/ 13 C' CSA tensor correlation spectra for GG and DKP, respectively. The spectra are clearly distinct from one another owing to the different relative orientations of the 1 H- 15 N dipolar and 13 C'

CSA tensors for the *trans* vs. *cis* peptide bond conformation. Remarkably, the corresponding simulated spectra shown in Fig. 4C and 4D, calculated for the *trans* and *cis* peptide bond conformations using the GG ¹³C' CSA tensor parameters, and ¹⁵N-¹H dipolar coupling magnitudes and relaxation rate constants for GG and DKP determined using the control experiments as discussed above, are in good agreement with the experimental data confirming the ability of the ¹H-¹⁵N dipolar/¹³C' CSA tensor correlation method to unambiguously differentiate between *trans* and *cis* peptide bonds.

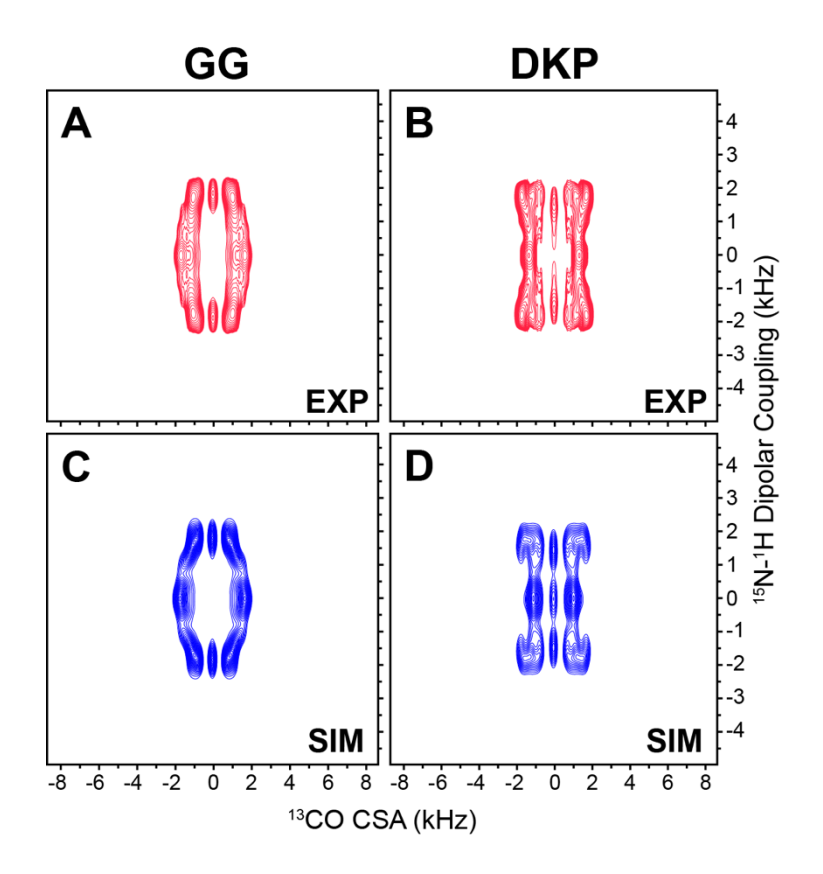


Figure 4. Experimental (A,B) and simulated (C,D) $^{1}\text{H-}^{15}\text{N}$ dipolar coupling/ $^{13}\text{C}'$ CSA correlation spectra for GG (A,C) and DKP (B,D). The experimental spectra were recorded in pseudo-3D fashion as described in the text, as 16 (τ_{DIP} , $^{1}\text{H-}^{15}\text{N}$ dipolar coupling) x 32 (τ_{CSA} , $^{13}\text{C}'$ CSA) data matrices with 100.8 μ s and 57.6 μ s dwell times in τ_{DIP} and τ_{CSA} , respectively, and 16 scans per FID. Spectra are drawn with lowest contours at ~20 times the root-mean-square (rms) noise level.

While the above approach could in principle be directly extended to larger peptides and proteins with overlapping 13 C' resonances by incorporating an additional 15 N chemical shift dimension (by independently incrementing t_1 , in addition to τ_{DIP} and τ_{CSA}) the resulting pseudo-4D experiment would be extremely time-consuming if recorded in a conventional manner. Two

possible approaches that may be considered to overcome this challenge and record residue-specific ^{1}H - ^{15}N dipolar/ $^{13}\text{C}'$ CSA tensor correlations within manageable measurement times include the use of: (1) non-uniform sampling for the ^{15}N chemical shift dimension [64,65] and (2) accordion spectroscopy [66,67] to simultaneously encode the ^{1}H - ^{15}N dipolar/ $^{13}\text{C}'$ CSA evolution in a time-shared manner. The latter approach was explored here by concurrently incrementing the τ_{DIP} and τ_{CSA} periods to yield correlated recoupled ^{1}H - ^{15}N dipolar/ $^{13}\text{C}'$ CSA lineshapes within a single frequency dimension.

To realize significant interplay between concurrently evolving tensorial interactions that is highly sensitive to their relative orientations, the product of the scaled interaction magnitude and evolution time must be comparable for the two interactions [22,26]. For the 1 H- 15 N dipolar coupling and 13 C′ CSA interactions being recoupled using the R18 $_1$ 7 and R14 $_2$ 3 sequences, respectively, this can be achieved by: (i) concurrently incrementing the R18 $_1$ 7 and R14 $_2$ 3 periods in units of two π pulses each resulting in the τ_{DIP} : τ_{CSA} ratio of 7:18 (we refer to this as a 1:1 accordion experiment, since both the R18 $_1$ 7 and R14 $_2$ 3 periods are incremented by the smallest possible unit of two π pulses) or (ii) incrementing the R18 $_1$ 7 period by four π pulses while concurrently incrementing the R14 $_2$ 3 period by two π pulses resulting in the τ_{DIP} : τ_{CSA} ratio of 7:9 (we refer to this as a 2:1 accordion experiment, since twice as many π pulses are applied during the R18 $_1$ 7 period versus the R14 $_2$ 3 period).

Fig. 5 shows the correlated ¹H-¹⁵N dipolar/¹³C' CSA frequency-domain lineshapes for GG and DKP obtained in pseudo-2D fashion by using the 1:1 and 2:1 accordion experiments described above. The distinctive experimental and corresponding simulated lineshapes—particularly for the 1:1 accordion experiments which yield a ~4 kHz splitting between the most intense features for GG and a ~2 kHz splitting for DKP—indicate that using this approach it is possible to readily distinguish between the *trans* and *cis* peptide bond conformations while employing measurement times that are 10-fold shorter than those needed for the corresponding

pseudo-3D experiments with independent ¹H-¹⁵N dipolar coupling and ¹³C' CSA dimensions (c.f., Fig. 4).

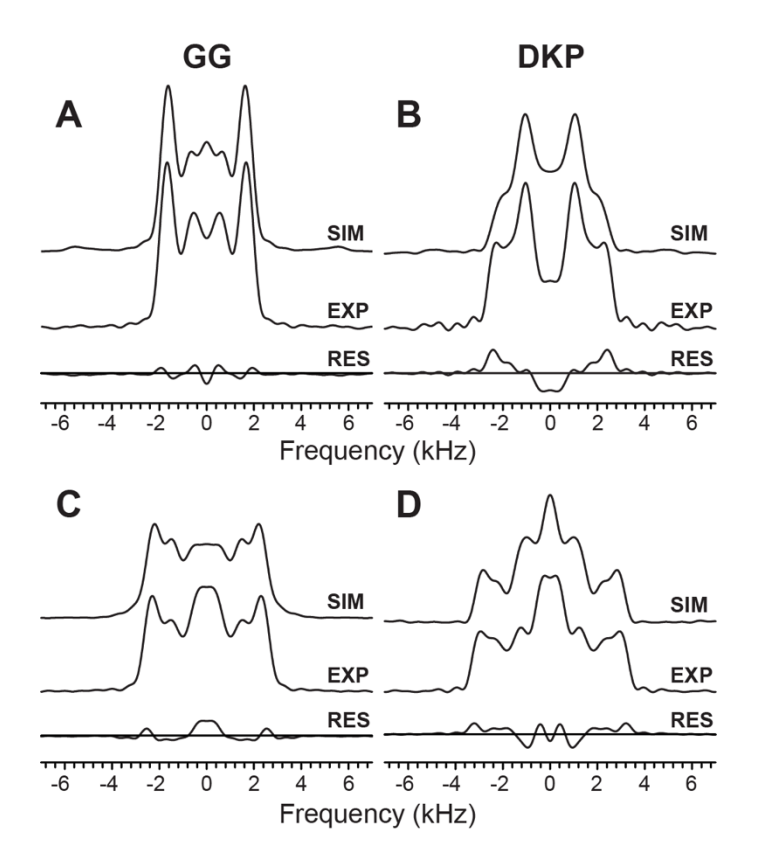


Figure 5. Experimental and best-fit simulated correlated ^{1}H - ^{15}N dipolar/ $^{13}\text{C}'$ CSA lineshapes for GG (A,C) and DKP (B,D) obtained in pseudo-2D fashion by using the 1:1 (A,B) and 2:1 (C,D) accordion experiments described in the text. For the 1:1 accordion experiments, 51 spectra were recorded in the $\tau_{\text{DIP}}/\tau_{\text{CSA}}$ dimension with increments of 11.2 μs for τ_{DIP} and 28.8 μs for τ_{CSA} and 16 scans per spectrum. Parameters were identical for the 2:1 accordion experiments, except that increments of 22.4 μs for τ_{DIP} and 28.8 μs for τ_{CSA} were used in the $\tau_{\text{DIP}}/\tau_{\text{CSA}}$ dimension. For each experiment the residuals are shown beneath the experimental and simulated lineshapes.

3.4. Tensor correlation experiments for proteins

Having established the ability of the ¹H-¹⁵N dipolar/¹³C' CSA tensor correlation experiments to unambiguously detect *cis* and *trans* peptide bond conformations in model peptides, we next used microcrystals of a globular 56-residue protein GB3 and Y145Stop prion protein amyloid fibrils as representative models to evaluate the applicability of these experiments to larger protein systems. Note that since no *cis* peptide bonds are expected to be present for either protein, this part of the study was primarily focused on issues related to

spectral sensitivity and ability of the tensor correlation experiments to clearly identify *trans* peptide bonds in these proteins in a residue-specific manner. The ¹H-¹⁵N dipolar/¹³C' CSA tensor correlation experiments for both protein samples were carried out as pseudo-3D's, consisting of two isotropic chemical shift dimensions (¹⁵N and ¹³C') for site resolution and an accordion dimension during which simultaneous evolution under the ¹H-¹⁵N dipolar coupling and ¹³C' CSA interactions was encoded as described above for GG and DKP (c.f., Fig. 5). Note that in comparison to the model peptides the use of the reduced-dimensionality accordion approach was particularly critical for the protein samples, where the collection of pseudo-3D spectra required measurement times ranging from ca. 2 to 6 days (i.e., if they were to be pursued the corresponding pseudo-4D's, consisting of two regularly sampled chemical shift dimensions and independent ¹H-¹⁵N dipolar coupling and ¹³C' CSA dimensions, would have required prohibitively long measurement times on the order of weeks to months).

Fig. 6 shows the experimental ${}^{1}H^{-15}N$ dipolar/ ${}^{13}C'$ CSA tensor correlation lineshapes obtained using the 1:1 accordion experiment for representative residues in GB3, with the complete set of lineshapes for all residues with resolved cross-peaks in the ${}^{15}N^{-13}C'$ spectrum provided in SI Fig. S2. First, we note that the spectral sensitivity is sufficient to yield high quality ${}^{1}H^{-15}N$ dipolar/ ${}^{13}C'$ CSA lineshapes. Furthermore, as expected, we find that all of the lineshapes display splittings of \sim 4 kHz between the most intense outer features and, on the whole, strongly resemble the corresponding *trans* peptide bond lineshape obtained for GG (c.f., Fig. 5A), in spite of relatively minor site-to-site variations in the central part of the lineshape that likely result from differences in ${}^{13}C'$ CSA parameters and relaxation properties [61-63]. In Fig. 7 we show the results of the same ${}^{1}H^{-15}N$ dipolar/ ${}^{13}C'$ CSA tensor correlation experiment performed for huPrP23-144 amyloid fibrils, which have previously been extensively investigated by our group using solid-state NMR methods [49,68-75] and are representative of more challenging protein assemblies in comparison to GB3 and other small microcrystalline

proteins. As was the case for GB3, we find that for all residues with resolved ¹⁵N-¹³C' correlations, the ¹H-¹⁵N dipolar/¹³C' CSA lineshapes exhibit prominent splittings of ~4 kHz between the most intense outer features that are characteristic of *trans* peptide bond conformation.

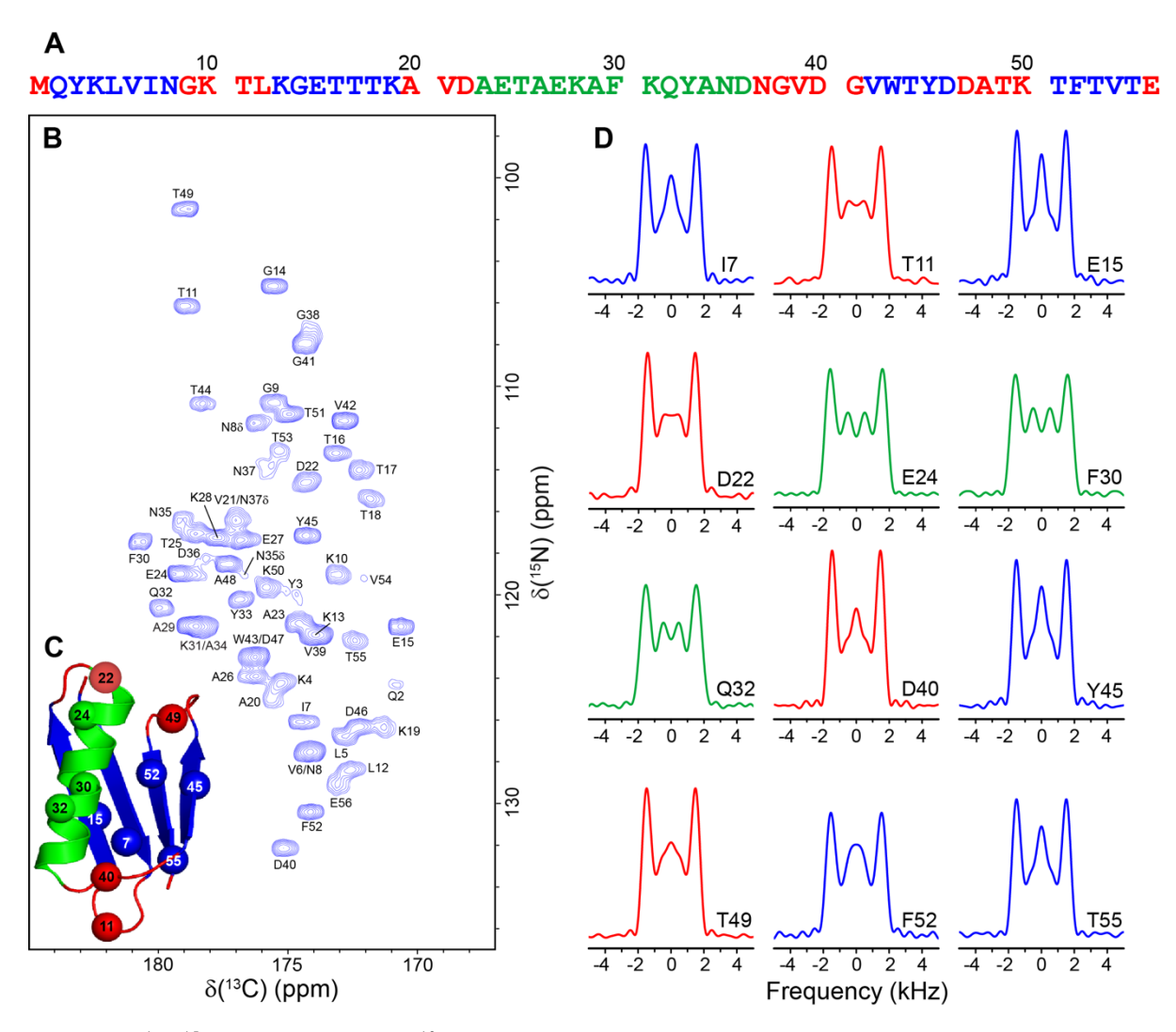


Figure 6. 1 H- 15 N dipolar coupling/ 13 C′ CSA tensor correlation experiments on GB3. (A) Amino acid sequence of GB3 with α-helix, β-sheet and loop residues shown in green, blue and red, respectively. (B) Two-dimensional 500 MHz 15 N- 13 C′ correlation spectrum of GB3 recorded at 9.921 kHz MAS rate as a 80* (1 t₁) x 1500* (13 t₂) data matrix with acquisition times of 28.44 ms and 30 ms in 1 t and 1 t₂, respectively, and 8 scans per FID. Cross-peaks are drawn with the lowest contour at ~12 times the rms noise level, and labeled with residue number according to the 15 N frequency [48]. (C) Structure of GB3 (PDB ID: 1P7E) [76] with locations of representative residues for which correlated 1 H- 15 N dipole/ 13 C′ lineshapes are shown indicated by spheres. (D) Experimental correlated 1 H- 15 N dipolar/ 13 C′ CSA lineshapes for representative residues in GB3 obtained in pseudo-3D fashion by using the 1:1 accordion experiment described in the text, where a set of 51 2D 15 N- 13 C′ correlation spectra with parameters listed in panel (B) was recorded with the $\tau_{\text{DIP}}/\tau_{\text{CSA}}$ dimension incremented by 11.2 μs for τ_{DIP} and 28.8 μs for τ_{CSA} . The lineshapes for the different residues are colored according to the secondary structure as indicated in panel (A) (see SI Fig. S2 for the complete set of experimental lineshapes).

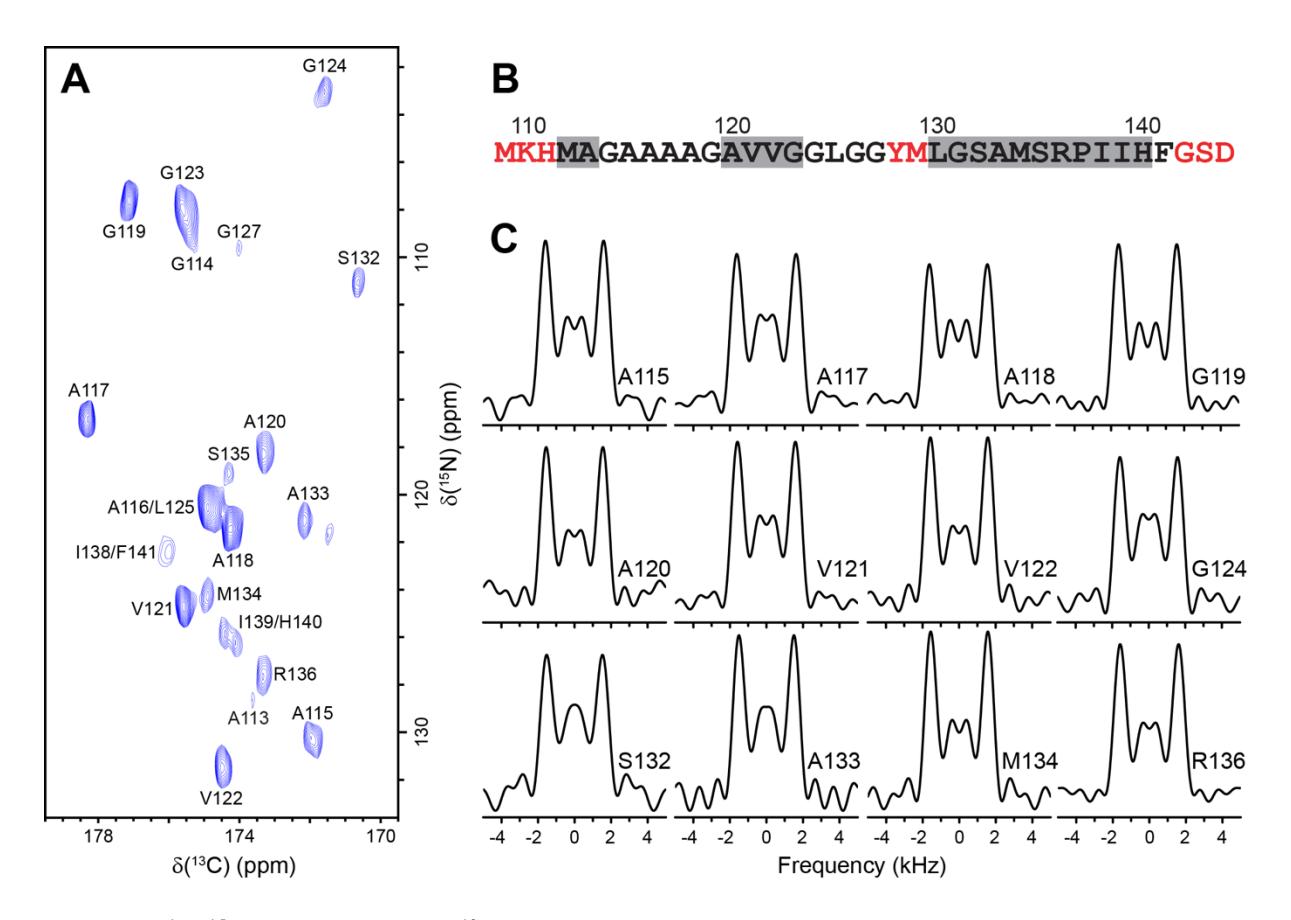


Figure 7. 1 H- 15 N dipolar coupling/ 13 C′ CSA tensor correlation experiments on huPrP23-144 amyloid fibrils. (A) Two-dimensional 500 MHz 15 N- 13 C′ correlation spectrum of huPrP23-144 fibrils prepared using the 1,3- 13 C-glycerol labeling scheme recorded at 9.921 kHz MAS rate as a 128* (t₁, 15 N) x 1500* (t₂, 13 C) data matrix with acquisition times of 11.43 ms and 30 ms in t₁ and t₂, respectively, and 16 scans per FID. Cross-peaks are drawn with the lowest contour at ~6 times the rms noise level, and labeled with residue number according to the 15 N frequency [68]. (B) Amino acid sequence for the huPrP23-144 amyloid core (amino acids 112-141) and several flanking residues. The most rigid residues are shown in black, flexible residues not detectable in CP-based spectra are shown in red, and predicted β-strands [72] based on TALOS-N analysis [77] are indicated by grey rectangles. (C) Experimental correlated 1 H- 15 N dipolar/ 13 C′ CSA lineshapes for representative residues in huPrP23-144 fibrils obtained in pseudo-3D fashion by using the 1:1 accordion experiment described in the text, where a set of 51 2D 15 N- 13 C′ correlation spectra with parameters listed in panel (A) was recorded with the $\tau_{\text{DIP}}/\tau_{\text{CSA}}$ dimension incremented by 11.2 μs for τ_{DIP} and 28.8 μs for τ_{CSA} .

4. Concluding remarks

In summary, we have demonstrated that the relative orientation of the amide ¹H-¹⁵N dipolar coupling and ¹³C' CSA tensors is highly sensitive to peptide bond conformation, and that it can be probed in uniformly ¹³C, ¹⁵N-labeled peptides and proteins by using multidimensional MAS solid-state NMR to readily distinguish between cis and trans peptide bonds in a residue-specific manner. The results obtained in this study for two model peptides, glycylglycine and 2,5-diketopiperazine, microcrystalline GB3 and huPrP23-144 amyloid fibrils indicate that these experiments should be broadly applicable to other peptides and microcrystalline and non-crystalline proteins. Of particular note in the context of these experiments, especially as they relate to larger proteins, is that accordion spectroscopy concepts can be employed to concurrently encode evolution under ¹H-¹⁵N dipolar coupling and ¹³C' CSA interactions within a single dimension. This reduces the experiment time by roughly an order of magnitude relative to that required with independent frequency dimensions, but without majorly sacrificing the information content. The ¹H-¹⁵N dipolar/¹³C' CSA tensor correlation experiments on proteins presented in this study were demonstrated at moderate MAS rates with ¹³C detection, and utilized samples containing on the order of 1 μmol of protein while requiring ~2-6 days of measurement time. Additionally, by employing extensions of these experiments based on approaches including faster MAS, paramagnetic-assisted condensed data collection and/or proton detection [78-86] it may be possible to further enhance the spectral sensitivity and resolution while concurrently reducing both the required sample amounts and measurement times. Given these considerations, applications to specific protein systems as well as larger scale survey type studies aimed at the characterization of the frequency of occurrence of cis peptide bonds in proteins can be envisioned.

Acknowledgments

This work was supported by the National Science Foundation (grants MCB-1243461 and MCB-1715174 to C.P.J.), the National Institutes of Health (grants R01GM094357, R01GM118664 and R01GM123743 to C.P.J.) and the Camille & Henry Dreyfus Foundation (Camille Dreyfus Teacher-Scholar Award to C.P.J.). We thank Dr. Subhradeep Paul for helpful discussions and Dr. Philippe Nadaud for assistance with GB3 sample preparation.

Supporting Information

Supporting information accompanies this paper at: ...

References

- [1] A. McDermott, Annu. Rev. Biophys. 38 (2009) 385-403.
- [2] R. Tycko, Annu. Rev. Phys. Chem. 62 (2011) 279-299.
- [3] A. Loquet, B. Habenstein, A. Lange, Acc. Chem. Res. 46 (2013) 2070-2079.
- [4] G. Comellas, C.M. Rienstra, Annu. Rev. Biophys. 42 (2013) 515-536.
- [5] S. Wang, V. Ladizhansky, Prog. Nucl. Magn. Reson. Spectrosc. 82 (2014) 1-26.
- [6] B.H. Meier, A. Bockmann, Curr. Opin. Struct. Biol. 30 (2015) 43-9.
- [7] M. Kaplan, C. Pinto, K. Houben, M. Baldus, Q. Rev. Biophys. 49 (2016) e15.
- [8] C.M. Quinn, T. Polenova, Q. Rev. Biophys. 50 (2017) e1.
- [9] M. Baldus, Prog. Nucl. Magn. Reson. Spect. 41 (2002) 1-47.
- [10] G. Pintacuda, G. Kervern, Top. Curr. Chem. 335 (2012) 157-200.
- [11] A. Bhaumik, C. Luchinat, G. Parigi, E. Ravera, M. Rinaldelli, CrystEngComm 15 (2013) 8639-8656.
- [12] C.P. Jaroniec, J. Magn. Reson. 253 (2015) 50-59.
- [13] R. Tycko, D.P. Weliky, A.E. Berger, J. Chem. Phys. 105 (1996) 7915-7930.
- [14] X. Feng, Y.K. Lee, D. Sandström, M. Eden, H. Maisel, A. Sebald, M.H. Levitt, Chem. Phys. Lett. 257 (1996) 314-320.
- [15] X. Feng, M. Eden, A. Brinkmann, H. Luthman, L. Eriksson, A. Gräslund, O.N. Antzutkin, M.H. Levitt, J. Am. Chem. Soc. 119 (1997) 12006-12007.
- [16] M. Hong, J.D. Gross, R.G. Griffin, J. Phys. Chem. B 101 (1997) 5869-5874.
- [17] P.R. Costa, J.D. Gross, M. Hong, R.G. Griffin, Chem. Phys. Lett. 280 (1997) 95-103.
- [18] M. Hong, J.D. Gross, W. Hu, R.G. Griffin, J. Magn. Reson. 135 (1998) 169-177.
- [19] Y. Ishii, K. Hirao, T. Terao, T. Terauchi, M. Oba, K. Nishiyama, M. Kainosho, Solid State Nucl. Magn. Reson. 11 (1998) 169-175.
- [20] B. Reif, M. Hohwy, C.P. Jaroniec, C.M. Rienstra, R.G. Griffin, J. Magn. Reson. 145 (2000) 132-141.
- [21] F.J. Blanco, R. Tycko, J. Magn. Reson. 149 (2001) 131-138.
- [22] C.M. Rienstra, M. Hohwy, L.J. Mueller, C.P. Jaroniec, B. Reif, R.G. Griffin, J. Am. Chem. Soc. 124 (2002) 11908-11922.

- [23] V. Ladizhansky, M. Veshtort, R.G. Griffin, J. Magn. Reson. 154 (2002) 317-324.
- [24] V. Ladizhansky, C.P. Jaroniec, A. Diehl, H. Oschkinat, R.G. Griffin, J. Am. Chem. Soc. 125 (2003) 6827-6833.
- [25] J.C.C. Chan, R. Tycko, J. Am. Chem. Soc. 125 (2003) 11828-11829.
- [26] C.P. Jaroniec, C.E. MacPhee, V.S. Bajaj, M.T. McMahon, C.M. Dobson, R.G. Griffin, Proc. Natl. Acad. Sci. USA 101 (2004) 711-716.
- [27] P.R. Costa, D.A. Kocisko, B.Q. Sun, P.T. Lansbury, R.G. Griffin, J. Am. Chem. Soc. 119 (1997) 10487-10493.
- [28] B.C. Hudson, A. Battigelli, M.D. Connolly, J. Edison, R.K. Spencer, S. Whitelam, R.N. Zuckermann, A.K. Paravastu, J. Phys. Chem. Lett. 9 (2018) 2574-2578.
- [29] G.N. Ramachandran, V. Sasisekharan, Adv. Prot. Chem. 23 (1968) 283-438.
- [30] M.S. Weiss, A. Jabs, R. Hilgenfeld, Nat. Struct. Biol. 5 (1998) 676.
- [31] A. Jabs, M.S. Weiss, R. Hilgenfeld, J. Mol. Biol. 286 (1999) 291-304.
- [32] D.C. Rees, M. Lewis, R.B. Honzatko, W.N. Lipscomb, K.D. Hardman, Proc. Natl. Acad. Sci. USA 78 (1981) 3408-3412.
- [33] K.W. Volz, D.A. Matthews, R.A. Alden, S.T. Freer, C. Hansch, B.T. Kaufman, J. Kraut, J. Biol. Chem. 257 (1982) 2528-2536.
- [34] M.S. Weiss, H.J. Metzner, R. Hilgenfeld, FEBS Lett. 423 (1998) 291-296.
- [35] T. Klabunde, S. Sharma, A. Telenti, W.R. Jacobs, J.C. Sacchettini, Nat. Struct. Biol. 5 (1998) 31-36.
- [36] B.L. Stoddard, S. Pietrokovski, Nat. Struct. Biol. 5 (1998) 3-5.
- [37] S.K. Sarkar, D.A. Torchia, K.D. Kopple, D.L. VanderHart, J. Am. Chem. Soc. 106 (1984) 3328-3331.
- [38] M. Schubert, D. Labudde, H. Oschkinat, P. Schmieder, J. Biomol. NMR 24 (2002) 149-154.
- [39] S. Neal, M. Berjanskii, H. Zhang, D.S. Wishart, Magn. Reson. Chem. 44 (2006) S158-S167.
- [40] Y. Shen, A. Bax, J. Biomol. NMR 46 (2010) 199-204.
- [41] K. Wüthrich, NMR of Proteins and Nucleic Acids, Wiley, New York, NY, 1986.
- [42] G. Hou, S. Paramasivam, I.J.L. Byeon, A.M. Gronenborn, T. Polenova, Phys. Chem. Chem. Phys. 12 (2010) 14873-14883.
- [43] R.E. Stark, L.W. Jelinski, D.J. Ruben, D.A. Torchia, R.G. Griffin, J. Magn. Reson. 55 (1983) 266-273.

- [44] C.J. Hartzell, M. Whitfield, T.G. Oas, G.P. Drobny, J. Am. Chem. Soc. 109 (1987) 5966-5969.
- [45] T.G. Oas, C.J. Hartzell, T.J. McMahon, G.P. Drobny, F.W. Dahlquist, J. Am. Chem. Soc. 109 (1987) 5956-5962.
- [46] T.F. Koetzle, W.C. Hamilton, R. Parthasarathy, Acta Crystallogr. B 28 (1972) 2083-2090.
- [47] Nonappa, K. Ahonen, M. Lahtinen, E. Kolehmainen, Green Chem. 13 (2011) 1203-1209.
- [48] P.S. Nadaud, J.J. Helmus, C.P. Jaroniec, Biomol. NMR Assign. 1 (2007) 117-120.
- [49] T. Theint, P.S. Nadaud, D. Aucoin, J.J. Helmus, S.P. Pondaven, K. Surewicz, W.K. Surewicz, C.P. Jaroniec, Nat. Commun. 8 (2017) 753.
- [50] D.J. States, R.A. Haberkorn, D.J. Ruben, J. Magn. Reson. 48 (1982) 286-292.
- [51] A.E. Bennett, C.M. Rienstra, M. Auger, K.V. Lakshmi, R.G. Griffin, J. Chem. Phys. 103 (1995) 6951-6957.
- [52] M. Baldus, A.T. Petkova, J. Herzfeld, R.G. Griffin, Mol. Phys. 95 (1998) 1197-1207.
- [53] F. Delaglio, S. Grzesiek, G.W. Vuister, G. Zhu, J. Pfeifer, A. Bax, J. Biomol. NMR 6 (1995) 277-293.
- [54] J.J. Helmus, C.P. Jaroniec, J. Biomol. NMR 55 (2013) 355-367.
- [55] M. Veshtort, R.G. Griffin, J. Magn. Reson. 178 (2006) 248-282.
- [56] M.H. Levitt, Symmetry-Based Pulse Sequences in Magic-Angle Spinning Solid-State NMR, in: D.M. Grant, R.K. Harris (Eds.), Encyclopedia of Nuclear Magnetic Resonance, Volume 9: Advances in NMR, Wiley, Chichester, 2002, pp. 165-196.
- [57] A. Brinkmann, M.H. Levitt, J. Chem. Phys. 115 (2001) 357-384.
- [58] X. Zhao, M. Eden, M.H. Levitt, Chem. Phys. Lett. 342 (2001) 353-361.
- [59] M.H. Levitt, J. Chem. Phys. 128 (2008) 052205.
- [60] G. Hou, I.-J.L. Byeon, J. Ahn, A.M. Gronenborn, T. Polenova, J. Chem. Phys. 137 (2012) 134201.
- [61] P.R. Markwick, M. Sattler, J. Am. Chem. Soc. 126 (2004) 11424-11425.
- [62] B.J. Wylie, L.J. Sperling, H.L. Frericks, G.J. Shah, W.T. Franks, C.M. Rienstra, J. Am. Chem. Soc. 129 (2007) 5318-5319.
- [63] Y. Wei, D.-K. Lee, A. Ramamoorthy, J. Am. Chem. Soc. 123 (2001) 6118-6126.
- [64] J.C. Hoch, M.W. Maciejewski, M. Mobli, A.D. Schuyler, A.S. Stern, Nonuniform Sampling in Multidimensional NMR, Wiley, Chichester, 2012.

- [65] S. Paramasivam, C.L. Suiter, G. Hou, S. Sun, M. Palmer, J.C. Hoch, D. Rovnyak, T. Polenova, J. Phys. Chem. B 116 (2012) 7416-7427.
- [66] G. Bodenhausen, R.R. Ernst, J. Magn. Reson. 45 (1981) 367-373.
- [67] G. Bodenhausen, R.R. Ernst, J. Am. Chem. Soc. 104 (1982) 1304-1309.
- [68] J.J. Helmus, K. Surewicz, P.S. Nadaud, W.K. Surewicz, C.P. Jaroniec, Proc. Natl. Acad. Sci. USA 105 (2008) 6284-6289.
- [69] J.J. Helmus, K. Surewicz, W.K. Surewicz, C.P. Jaroniec, J. Am. Chem. Soc. 132 (2010) 2393-2403.
- [70] J.J. Helmus, K. Surewicz, M.I. Apostol, W.K. Surewicz, C.P. Jaroniec, J. Am. Chem. Soc. 133 (2011) 13934-13937.
- [71] E.M. Jones, B. Wu, K. Surewicz, P.S. Nadaud, J.J. Helmus, S. Chen, C.P. Jaroniec, W.K. Surewicz, J. Biol. Chem. 286 (2011) 42777-42784.
- [72] T. Theint, P.S. Nadaud, K. Surewicz, W.K. Surewicz, C.P. Jaroniec, Biomol. NMR Assign. 11 (2017) 75-80.
- [73] D. Aucoin, Y. Xia, T. Theint, P.S. Nadaud, K. Surewicz, W.K. Surewicz, C.P. Jaroniec, J. Struct. Biol. (2018) published online, doi: 10.1016/j.jsb.2018.04.002.
- [74] M.D. Shannon, T. Theint, D. Mukhopadhyay, K. Surewicz, W.K. Surewicz, D. Marion, P. Schanda, C.P. Jaroniec, ChemPhysChem (2018) published online, doi: 10.1002/cphc.201800779.
- [75] T. Theint, Y. Xia, P.S. Nadaud, D. Mukhopadhyay, C.D. Schwieters, K. Surewicz, W.K. Surewicz, C.P. Jaroniec, J. Am. Chem. Soc. 140 (2018) 13161-13166.
- [76] T.S. Ulmer, B.E. Ramirez, F. Delaglio, A. Bax, Journal of the American Chemical Society 125 (2003) 9179-9191.
- [77] Y. Shen, A. Bax, J. Biomol. NMR 56 (2013) 227-241.
- [78] N.P. Wickramasinghe, S. Parthasarathy, C.R. Jones, C. Bhardwaj, F. Long, M. Kotecha, S. Mehboob, L.W.M. Fung, J. Past, A. Samoson, Y. Ishii, Nat. Methods 6 (2009) 215-218.
- [79] R. Linser, V. Chevelkov, A. Diehl, B. Reif, J. Magn. Reson. 189 (2007) 209-216.
- [80] S. Laage, J.R. Sachleben, S. Steuernagel, R. Pierattelli, G. Pintacuda, L. Emsley, J. Magn. Reson. 196 (2009) 133-141.
- [81] I. Bertini, L. Emsley, M. Lelli, C. Luchinat, J. Mao, G. Pintacuda, J. Am. Chem. Soc. 132 (2010) 5558–5559.
- [82] P.S. Nadaud, J.J. Helmus, I. Sengupta, C.P. Jaroniec, J. Am. Chem. Soc. 132 (2010) 9561-9563.

- [83] K. Yamamoto, J. Xu, K.E. Kawulka, J.C. Vederas, A. Ramamoorthy, J. Am. Chem. Soc. 132 (2010) 6929-6931.
- [84] M. Tang, D.A. Berthold, C.M. Rienstra, J. Phys. Chem. Lett. 2 (2011) 1836-1841.
- [85] D. Mukhopadhyay, P.S. Nadaud, M.D. Shannon, C.P. Jaroniec, J. Phys. Chem. Lett. 8 (2017) 5871-5877.
- [86] L.B. Andreas, T. Le Marchand, K. Jaudzems, G. Pintacuda, J. Magn. Reson. 253 (2015) 36-49.